Optofluidic microengine in a dynamic flow environment via self-induced back-action

Shi, Yuzhi; Zhu, Tongtong; Nguyen, Kim Truc; Zhang, Yi; Xiong, Sha; Yap, Peng Huat; Ser, Wee; Wang, Shubo; Qiu, Cheng-Wei; Chan, C. T.; Liu, Ai Qun

2020

Shi, Y., Zhu, T., Nguyen, K. T., Zhang, Y., Xiong, S., Yap, P. H., Ser, W., Wang, S., Qiu, C., Chan, C. T. & Liu, A. Q. (2020). Optofluidic microengine in a dynamic flow environment via self-induced back-action. ACS Photonics, 7(6), 1500-1507. https://dx.doi.org/10.1021/acsphotonics.0c00295

https://hdl.handle.net/10356/151474

https://doi.org/10.1021/acsphotonics.0c00295

Optofluidic Micro-Engine in A Dynamic Flow Environment *via* Self-Induced Back-Action

Yuzhi Shi[1], Tongtong Zhu[2], Kim Truc Nguyen[1], Yi Zhang[3], Sha Xiong[4], Peng Huat Yap[5], Wee Ser[1], Shubo Wang[6], Cheng-Wei Qiu[7], C. T. Chan[8*], and Ai Qun Liu[1*]

[1] *School of Electrical and Electronic Engineering, Nanyang Technological University, Singapore 639798*

[2] *School of Optoelectronic Engineering and Instrumentation Science, Dalian University of Technology, Dalian, 116024, China*

[3] *School of Mechanical and Aerospace Engineering, Nanyang Technological University Singapore 639798*

[4] *School of Automation, Central South University, Changsha 410083, China*

[5] *Lee Kong Chian School of Medicine, Nanyang Technological University, Singapore 308232*

[6] *Department of Physics, City University of Hong Kong, Tat Chee Avenue, Kowloon, Hong Kong SAR, China*

[7] *Department of Electrical and Computer Engineering, National University of Singapore, Singapore 117583*

[8] *Department of Physics, The Hong Kong University of Science and Technology, Clear Water Bay, Hong Kong, China*

**Corresponding Authors: C. T. Chan (phchan@ust.hk); Ai Qun Liu (eaqliu@ntu.eud.sg)*

ABSTRACT

Most existing optofluidic particle engines only operate in a static environment. Here, we present a four-energy-state optofluidic micro-engine that operates stably in a dynamic flow environment, a function unattainable by existing systems due to the disturbance of fluidic drag force. This micro-engine is powered synergistically by both the optical force and fluidic drag force, and exploits the intriguing behavior of the particle in an asymmetric two-dimensional light interference pattern under the self-induced back-action (SIBA) effect. The mechanism of the micro-engine is studied in detail, and micro-engine comprising of a single cell and a cell-particle complex have been demonstrated. Our optofluidic micro-engine is the first of its kind to operate in the dynamic flow environment, and provides a new platform to study of single cell dynamics and cell-particle or cell-cell interactions in the dynamic fluidic environment.

KEYWORDS: self-induced back-action, optofluidic engine, optical pulling force, optical binding, optical trapping

Light-driven micro-engines, which convert photon energy into mechanical energy of a microparticle via light-matter interactions, have found a wide range of biomedical and optomechanical applications.[1-10] Most existing light-driven micro-engines only operate in a static environment in which the optical force is the sole dominant force,[1, 5, 11-16] and the potential wells are not disturbed by the fluidic drag force. Examples include the light-driven plasmonic motor,[1] optical spinning motor,[2] light-controlled stochastic heat engine,[3] piston-like photophoretic motor,[9] and the recent lamb wave engine driven by a pulsed light source.[17] Up to date, no light-driven micro-engines could operate stably in a dynamic flow environment because the fluidic drag force would disturb the potential wells and destabilize the micro-engine.[18] As a result, the optical extinction force must be constantly adjusted against the fluidic drag force in order for the particle to maneuver along closed trajectories.[6] Nevertheless, this optofluidic system is not considered a micro-engine because the particle trajectory is stochastic.

We now demonstrate an optofluidic system with asymmetric interference patterns in which fluidic drag force and optical force power a micro-engine synergistically. This optofluidic system takes advantage of the self-induced back-action[19-21] (SIBA) of microparticles in the asymmetric light pattern to create a four-energy-level micro-engine that operates stably in the dynamic flow environment. The SIBA effect becomes prominent when the particle size is comparable to the size of the hotspot. Under such conditions, the particle could reshape the light pattern on its own or interact with the preconfigured structure.[21] Consequently, the optical force could be the strongly enhanced or suppressed, even having sign reversed, etc. The SIBA effect has been used to study the force in the nano-hole[19] and the photonic crystal[20] tapping systems.[22] Nonetheless, this intriguing phenomenon is often overlooked in many optical trapping systems. In our system, the SIBA effect does not only flatten the potential well to facilitate the particle hopping, but also

generates an optical pulling force[9, 20, 23-26] to facilitate the back flushing together with the fluidic drag force. This work, for the first time, demonstrates a four-energy-level light-driven particle micro-engine that is powered synergistically by optical force and fluidic drag force in the dynamic flow environment, and opens a new avenue for optofluidic manipulation.

The schematics of the optofluidic micro-engine is shown in Figure 1a. Distinct from conventional optical trapping systems in which particles stay in the valley of the potential well, the optofluidic micro-engine has four energy levels that resembles the power cycle of classical macroscopic four-stroke engines.[3, 27] The light is configured into a subtly asymmetric interference pattern in which a particle is driven synergistically by both optical force and fluidic drag force along a closed trajectory. Among the three adjacent hotspots in the light interference pattern, the primary hotspot with the highest intensity is located on the left, and the two secondary hotspots are located on the right. The secondary hotspots with higher and lower intensities are called the major and minor secondary hotspots, respectively. Starting from the primary hotspot, the optical extinction force pushes the particle from Energy State 1 (E_1) towards E_2 along the direction of light propagation until the particle rests temporarily at the zero-net-force location E_2 where the optical force is balanced by the fluidic drag force. Due to Brownian motion, the particle would hop from E_2 to E_3 in the adjacent major secondary hotspot. This hopping motion is facilitated by the SIBA effect to flatten the potential well (Supporting Information, section 1). The particle at E_3 is then flushed with the flow to E_4, and eventually it hops back to E_1 to re-initiate another engine cycle.

From the starting point (E_1) to the first hopping point (E_2), the net force is dominated by the optical force which does a positive work to the particle (charge stroke 1) as shown in Figure 1a-c. To generate an engine cycle, the potential well at E_2 must be shallow enough for the particle to escape, and the potential well at E_3 must be deep enough to retain the particle. This ccondition

may seems to imply that the light intensity at E_3 is higher than that at E_2, hence the particle would be pushed away from E_3 hence unable to complete an engine cycle. In fact, thanks to SIBA, the optical force at E_3 is smaller than that at E_2 or even reverses its direction, resulting in an optical pulling force instead of pushing force on the particle in this specific case. This optical pulling force subsequently works synergistically with the fluidic drag force to flush the particle from E_3 to E_4 against the direction of light propagation. Therefore, E_2 has the highest potential energy in the engine cycle. As the particle hops from the E_2 to E_3, it releases energy (power stroke 1) and a negative work is done by the particle. As the particle is flushed from E_3 to the second hopping point (E_4) which has a higher energy, the combined force does a positive work on the particle (charge stroke 2). Due to the optical gradient force, the particle hops from E_4 to the lower-energy State E_1, thereby releasing energy and generating the second power stroke. While the mechanisms of power generation are different, our SIBA micro engine and the macroscopic engine do have some commonalities in terms of the power cycle. Both engines store energy in two strokes (charge stroke) and release energy in the other two strokes (power stroke) during one complete engine cycle.

In another scenario with exceedingly high laser power, as the particle hops from the primary hotspot to the major secondary hotspot (E_{22} to E_{32}) (Figure 1b), it is pushed away along the direction of light propagation instead of being flushed back due to the strong optical force in the secondary hotspot. Therefore, no engine cycle is generated. The energy levels of this scenario are shown in Figure 1d.

The asymmetric light interference pattern is key to realizing the optofluidic engine cycle.[6] When the waist of the Gaussian beam from an optical fiber is located 150 μm away from the left edge of the microlens and the axis of the beam is aligned with the principle axis of the microlens,

the light rays generate a symmetric interference pattern in the optofluidic channel, giving the particle in the primary hotspot an equal chance to hop to either one of the two secondary hotspots. To precisely control the direction of particle hopping, we propose asymmetric light patterns generated using two methods shown in Supporting Information, section 2. One way is to shift the axis of the beam away from the principle axis of the microlens by a distance Δh along the y direction. Consequently, the interference pattern behind the microlens has a primary hotspot on the left and two asymmetric secondary hotspots with stronger (major secondary hotspot) and weaker (minor secondary hotspot) intensities on the right. Alternatively, tilting the beam axis with a certain angle (e.g., 1° or 2°) also generates a similar asymmetric light interference pattern. When the angle θ is positive, the particle hops clockwise among the hotspots, and *vice versa*. The asymmetric interference pattern ensures that the particle in the primary hotspot would only hop into the major secondary hotspot and cycle along a well-defined trajectory, a function unattainable by previously reported systems.[6, 28] Meanwhile, by modulating the incident angle of the laser beam, the direction of the cyclic motion can be easily tuned between clockwise and anti-clockwise, which is more flexible than other optics-induced cyclic motions. For example, plasmonic thermal tweezers are able to induce particle cyclic motion but unable to change the direciton.[18]

Different particles may experience distinctive SIBA effects in terms of the direction of optical force and the shape of potential well, thereby resulting in drastically different behaviors in the asymmetric interference pattern (Figure 2). For example, the optical scattering force prevails over the optical gradient force on the 1-μm particle residing at the edge of the primary hotspot as shown in Figure 2a. In contrast, the optical gradient force dominates and generates a pulling force for the 100-nm nanoparticle in Figure 2b. This is because the optical gradient force for a Rayleigh nanoparticle is proportional to R^3 (R is the radius of the particle), while the optical gradient force

is proportional to R^6. Therefore, the optical gradient force is normally larger than the optical scattering force for nanoparticles. In the major secondary hotspot, the 100-nm nanoparticles can experience a strong forward scattering induced optical pulling force as shown in Figure 2c. The strong forward scattering results from the tilted light rays due to the refraction of the microlens, which originates in a way similar to the origin of optical pulling force from the Bessel beam. The strong backward scattering can balance the forward scattering for the 1-μm particle as shown in Figure 2d.

Let us consider two scenarios as the particles hop from the primary hotspot to the major secondary hotspot. In one scenario shown in Figure 2e, the balance position of the particle (P1) in the main hotspot is located at x = 11.8 μm (the right edge of the microlens is defined as x = 0) when the laser power is 150 mW, and the flow velocity is 7.1 μm/s. The optical forces in the x-direction F_x from -4 to 4 μm along the y axis is shown in Figure 2f. The optical forces on the 100-nm and 1-μm particles have opposite signs in P1 as calculated by the FDTD method. This phenomenon occurs because the 100-nm nanoparticle is dominated by the optical gradient force (pulling force), whereas the 1-μm particle is dominated by the radiation force (pushing force). Since Rayleigh theory predicts that the optical extinction force on a nanoparticle is proportional to the light intensity, which is also known as the Perturbative theory[19] (Supporting Information, section 3), the calculated optical force on the 100-nm particle is positive regardless of the location of the particle as shown in Figure 2f where the dot curve matches the profile of the light intensity. The optical force profile from the Perturbative theory is different from the rigorous FDTD method based on Minkowski stress tensor.[29] Both the 100-nm and 1-μm particles experience the pulling force in the major secondary hotspot because of the strong forward scattering on the particles in

P2. The shapes of potential wells for the two particles calculated by both FDTD and Perturbative methods are similar to the intensity profile of the two hotspots as shown in Figure 2g.

In the other scenario (P3 to P4, also the case for E_2 to E_3 in the cycle) in Figure 2h, when the balance position of both particles in the primary hotspot is at x = 16.3 μm (P3), the direction of F_x on both particles in the primary hotspot calculated by FDTD at y = -0.4 μm remains the same with that in the previous scenario shown in Figure 2f. Since the intensity at P4 is much higher than that of P2, the optical-radiation-induced pushing effect on the 1-μm particle becomes large enough to neutralize the forward-scattering-induced pulling force, generating a net force of ~ 0 as shown in Figure 2i. The shape of the potential well calculated by both methods (FDTD and Perturbative) for the 100-nm nanoparticle matches the light intensity profile as shown in Figure 2j. However, the potential well of the primary hotspot is completely overwhelmed by the SIBA effect in the presence of the 1-μm particle, making it much easier for the 1-μm particle to hop to the major secondary hotspot. This phenomenon happens because the size of the 1-μm particle is close to the size of the major secondary hotspot, which imposes an attractive force on the particle due to SIBA effect to pull the particle away from the primary hotspot. Subsequently, once the 1-μm particle hops into the major secondary hotspot, an optical pulling force generated due to the SIBA effect neutralizes the pushing force, thereby allowing the fluidic drag force to flush the particle against the direction of light propagation even though the light intensity at P4 is high than that at P3. Therefore, SIBA enables the micro-engine by generating optical pulling force and reshaping the potential wells. The Poynting vectors (Supporting Information, section 4) clearly show an optical pulling force induced by the strong forward scattering and an optical pushing force induced by the normal scattering and light focusing. The refractive indices of the 100-nm and 1-μm particle are both 1.38. It is noted that the potential well of the 100-nm nanoparticle is much shallower than that

of the 1-μm particle (multiplied by a factor of 10^4 in Figure 3). This shallow potential well is not strong enough to trap the 100-nm nanoparticles.

The two-dimensional (2D) potential landscapes combining all forces, including optical forces F_{opt} and fluidic drag force F_{drag}, are shown in Figure 3. The optical force in the conventional optical tweezers is a conservative force, while the fluidic drag force, which represents the fluidic friction, is a non-conservative force. The combined two-dimensional force field is hence non-conservative. Because the trajectory of the particle is fixed (rectangle) and the two-dimensional force field is non-conservative, the potential energy at each point is calculated by defining the energy at the original point (e.g., point (0, -4) in Figure 2e) of the force map to be 0 (see illustration in Supporting Information, section 5). The total force in each point can be defined as $F(x, y) = F_{opt}(x, y) + F_{drag} = F_{opt}(x, y) + 6\pi\eta a v$, where η and v are the viscosity and the velocity of the flow, respectively. We then integrate the forces along the y-direction to obtain the $U(0, y)$. The potential energy in the arbitrary point (x, y) can be expressed as $U(x,y) = U(0,y) + \int_0^x F(X,y)\,dX$. It is noted that this definition of potential energy here may not be suitable for all two-dimensional force fields, for example those with chaotic trajectories of particles or with irregularly distributed non-conservative forces. The method here illustrates the energy transfer well because the particle moves along a rectangle trajectory and the force in the y-direction is mainly contributed by the conservative optical gradient force.

The particle in the valley (E_1) of the potential well is pushed to the plateau (E_2) by the optical extinction force when the laser power is 300 mW. The SIBA effect results in an overall negative force in the y-direction, which facilitates the particle hopping from the primary hotspot (E_2) to the major secondary hotspot (E_3) and releases energy during the hopping. Subsequently,

the optical pulling force and fluidic drag force raise the particle to a higher energy E_4 as discussed in Figure 2. As the particle gradually moves back towards the primary hotspot with the flow stream, the potential well of the primary hotspot becomes deeper, and the particle stores energy during this process. In the end, the particle hops into the primary hotspot and releases energy. The energy drops into E_1 and a new cycle is re-initiated. When the laser power is too high (e.g., 900 mW), the particle would be pushed away by the optical scattering forces as shown in Supporting Information, section 4.

The experimental demonstration of the micro-engine with *Cryptosporidium* oocysts is shown in Figure 4. The oocyst is able to cycle on its own (Figure 1a) or together with a nanoparticle as an oocyst-particle complex (Figure 4a). The cyclic motion of a single *Cryptosporidium* oocyst micro-engine is shown in Figure 4b. The oocyst was initially pushed to the right by the optical force at $t = 0$, and reached the force-balancing position at $t = 0.9$ s. It took the oocyst 1.3 s to hop to the adjacent potential well in the secondary hotspot, where the optical force was not strong enough to compete with the fluidic drag force due to the SIBA effect. As a result, the oocyst was flushed back by the fluidic drag force and hopped back to the primary hotspot to re-initiate a new engine cycle. The micro-engine with the oocyst-particle complex showed a shorter cycle perimeter and period (Figure 4c) compared to the single-oocyst micro-engine. This is because the optical force increases more rapidly than the fluidic drag force as the equivalent size of the particle increases. Thus, the optical gradient force attracts the complex and cause the particle to move from E_4 to E_1 more easily and quickly. The size and the refractive index of the silica particle attached to the oocyst were 1 μm and 1.46, respectively. The nanoparticle "tail" of the complex always pointed to the positive x-direction due to the optical alignment of the oblong hotspot. In the experiment, the highest intensity of the light pattern is

approximately 10^{10} W/m^2 which is at least 2 orders magnitude lower than those reported in optical tweezing systems for virus[30, 31] or RNA[32] trapping, yet no significant temperature change nor convective flow is observed in those systems. Our all-dielectric SIBA-based system is distinct from the plasmonic optical tweezers in which the laser generates huge amount of heat and induces the convective flow.[33, 34] The biological entities are able to remain intact and viable in the laser with an intensity 10^{10} W/m^2 laser power.[30-32] The oocyst incubated with antibodies can catch the streptavidin particle easily in the laser beam.

The recorded *y*-coordinates of a single oocyst micro-engine in Figure 4d showed a cyclic motion with a charge stroke by laser (E_1 to E_2) followed by the first power stroke (E_2 to E_3), another charge stroke by flow (E_3 to E_4) and the second power stroke (E_4 to E_1) in each cycle. The period of the cycle was around 6-7 s because the Brownian-motion-initiated hopping had a random interval. The micro-engine relies on the synergy of the optical forces and fluidic forces which are controlled by the laser power and flow velocities, respectively. The optical gradient force in the *y*-direction is strong enough to confine the particle or cell in the cycle. Therefore, the micro-engine can stably run for hours. The micro-engine has almost identical movement in each cycle (only 5 cycles are shown) as shown in Figure 4d. The displacement of the particle and the work done by the optical force and fluidic drag force in one cycle are shown in Figure 4e. The net forces exerted on the particle is estimated as $6\pi\eta a v$,[35] where η is the viscosity of the fluid, a and v are the radius and velocity of the particle, respectively. The cycle distance is over 12 μm, and the particle velocity is between -5 to 10 μm/s. The work done by the optical force and the laser force in the two charge strokes is around 2×10^{-18} *J* by integrating the force along the moving trajectory, which is expressed as $W = \int F_x dx$. Though the power is not high compared to other micros-engines, it is the first attempt to build an optofluidic micro-engine with four energy levels

in a dynamic flow environment by harnessing both the optical and fluidic forces and exploiting the intriguing behavior of particles under the SIBA effect.[26] This optofluidic micro-engine provides a way of manipulating particles in the dynamic flow environment such as microfluidic bioreactors that are constantly under perfusion. Such a function is unattainable by other micro-motors which can only operate in the static environment, e.g. particle rotation by an optical beam carrying orbital angular momentum.

In summary, we have developed an optofluidic micro-engine with an asymmetric light interference pattern. The optofluidic micro-engine operates stably in the dynamic flow environment by harnessing both the optical and fluidic forces. The four-energy-level micro-engine relies on the synergy of multiple effects, including the pushing and pulling by optical forces, flushing by the fluidic drag force, and the hopping between potential wells. Morevore, the SIBA effect empowers the engine in two ways: it does not only flatten the potential well for easy particle hopping, but also generates optical pulling forces to facilitate the backward motion in synergy with the fluidic drag force. We demonstrated optofluidic micro-engines comprising a single *Cryptosporidium* oocyst or an oocyst-particle complex in the microfluidic channel. These micro-engines might provide a new platform for the study of single cell dynamics and cell-particle or cell-cell interactions in the dynamic fluidic environment.

METHODS

Optofluidic chip and sample preparation. The optofluidic chip consisted of a microfluidic channel with three inlets and two outlets.[36] The microchannel had dimensions of length L = 1000 μm, width W = 70 μm and height H = 70 μm. The three injected flow streams were all phosphate-

buffered saline (PBS) solution with particles and oocysts in the core flow stream. A microlens was made from polydimethylsiloxane (PDMS) and placed at the edge of the microchannel. A 532 nm single mode optical fibre was inserted into a groove with 1° to the microlens axis. A tilted discrete optical interference pattern was generated on the right of the microlens for the oocyst cycle. *Cryptosporidium parvum* oocysts (Waterborne Inc.) were stored at 4 °C with a concentration of 10^8 oocysts/mL. The oocyst stock solution was diluted to the desired concentration for each experiment. The oocysts were rinsed three times and centrifuged at 10000×g for 3 min. The supernatant was discarded, and the resulting pellet was re-suspended in PBS. The suspension of *C. parvum* oocysts was incubated with biotinylated anti-*Cryptosporidium parvum* oocysts antibody (mAb) (Waterborne Inc.) in a humidified chamber protected from light for 90 minutes. Then the suspension was washed with sterile PBS (pH 7.4). The concentration of the biotin-labelled *C. parvum* oocysts used in the hopping experiment was 10^4 oocysts/mL. Streptavidin coated silica microparticles (Bangs laboratories Inc.) with a diameter of 1 μm were suspended in PBS and the concentration was adjusted to 10^6 particles/mL.

Simulation of light field and optical forces. The interference fields created by a Gaussian beam illuminating the micro-lens were modelled using the commercial software Lumerical. The *z*-polarized Gaussian beam with NA = 0.12 and wavelength of 532 nm was placed 150 μm away from the edge of the micro-lens (see Supplementary Information). When the beam illuminated the micro-lens with an incident angle 1°, an interference field in the *x*-*y* plane could be created. To save the computer memory, a new light source in the *y*-*z* plane was defined right after the lens in Lumerical. The light source was exported to a Matlab file (source.mat) and used as a new light source for the simulation of optical forces on the particles. The optical force simulation using

FDTD method was also conducted in Lumerical based on the time-averaged Maxwell stress tensor, which can be expressed as

$$\langle \boldsymbol{F} \rangle = \oint_S \langle \overleftrightarrow{T} \rangle \, d\boldsymbol{S}, \tag{1}$$

where the integration is performed over a closed surface near the object, and $\langle \cdot \rangle$ means the time average operation. The stress tensor using here is Minkowski form and expressed as

$$\langle T_{ij} \rangle = \frac{1}{2} Re \left[\varepsilon E_i E_j^* + \mu H_i H_j^* - \frac{1}{2} (\varepsilon E \cdot E^* + \mu H \cdot H^*) \delta_{ij} \right], \tag{2}$$

where ε and $\boldsymbol{\mu}$ are the relative permittivity and relative permeability of the medium, respectively. We compare the integration of Minkowski stress tensor over a cube and a sphere surface as shown in Supporting Information, section 3. The two integration methods agree each other. We choose the integration over a cube which is 15 nm away from the surface of the particle for a faster computing and easy operation.

The force in each point (x, y) in the two-dimensional force field is defined as $F(x, y)$. The potential energy $U(x, y)$ in Fig. 3 is then be defined as

$$U(x, y) = \int_0^y F(0, Y) dY + \int_0^x F(X, y) dX , \tag{3}$$

ASSOCIATED CONTENT

Supporting information

The Supporting Information is available free of charge at

Additional materials of the theory of light field, optical forces and potential wells. Supporting experimental results of optical binding and particle dynamics (PDF)

AUTHOR INFORMATION

Corresponding Author

C. T. Chan – Department of Physics, Hong Kong University of Science and Technology, Hong Kong, China; Email: phchan@ust.hk

Ai Qun Liu – School of Electrical and Electronic Engineering, Nanyang Technological University, Singapore 639798; Email: eaqliu@ntu.edu.sg

Notes

The authors declare no competing financial interest.

ACKNOWLEDGMENTS

This work is supported by National Research Foundation under the Competitive Research Program (NRF-CRP13-2014-01) and Singapore Ministry of Education (MOE) Tier 3 grant (MOE2017-T3-1-001). C.T.C. acknowledges support by Hong Kong RGC through grants 16303119 and AoE/P-02/12.

REFERENCES

1. Liu, M.; Zentgraf, T.; Liu, Y.; Bartal, G.; Zhang, X. Light-driven nanoscale plasmonic motors. *Nat. Nanotechnol.* **2010,** *5*, 570-573.

2. Friese, M. E. J.; Nieminen, T. A.; Heckenberg, N. R.; Rubinsztein-Dunlop, H. Optical alignment and spinning of laser-trapped microscopic particles. *Nature* **1998,** *394* (6691), 348-350.

3. Blickle, V.; Bechinger, C. Realization of a micrometre-sized stochastic heat engine. *Nat. Phys.* **2011,** *8*, 143-146.

4. Kelemen, L.; Valkai, S.; Ormos, P. Integrated optical motor. *Appl. Opt.* **2006,** *45* (12), 2777-2780.

5. Maggi, C.; Saglimbeni, F.; Dipalo, M.; De Angelis, F.; Di Leonardo, R. Micromotors with asymmetric shape that efficiently convert light into work by thermocapillary effects. *Nat. Commun.* **2015,** *6*, 7855.

6. Shi, Y. Z.; Xiong, S.; Zhang, Y.; Chin, L. K.; Chen, Y. Y.; Zhang, J. B.; Zhang, T. H.; Ser, W.; Larson, A.; Hoi, L. S.; et al. Sculpting nanoparticle dynamics for single-bacteria-level screening and direct binding-efficiency measurement. *Nat. Commun.* **2018,** *9* (1), 815.

7. Shi, Y.; Xiong, S.; Chin, L. K.; Zhang, J.; Ser, W.; Wu, J.; Chen, T.; Yang, Z.; Hao, Y.; Liedberg, B.; et al. Nanometer-precision linear sorting with synchronized optofluidic dual barriers. *Sci. Adv.* **2018,** *4* (1), eaao0773.

8. Shi, Y. Z.; Xiong, S.; Chin, L. K.; Yang, Y.; Zhang, J. B.; Ser, W.; Wu, J. H.; Chen, T. N.; Yang, Z. C.; Hao, Y. L.; et al. High-resolution and multi-range particle separation by microscopic vibration in an optofluidic chip. *Lab Chip* **2017,** *17* (14), 2443-2450.

9. Lu, J.; Yang, H.; Zhou, L.; Yang, Y.; Luo, S.; Li, Q.; Qiu, M. Light-Induced Pulling and Pushing by the Synergic Effect of Optical Force and Photophoretic Force. *Phys. Rev. Lett.* **2017,** *118* (4), 043601.

10. Kaynak, M.; Ozcelik, A.; Nourhani, A.; Lammert, P. E.; Crespi, V. H.; Huang, T. J. Acoustic actuation of bioinspired microswimmers. *Lab Chip* **2017,** *17* (3), 395-400.

11. Magallanes, H.; Brasselet, E. Macroscopic direct observation of optical spin-dependent lateral forces and left-handed torques. *Nat. Photonics* **2018,** *12* (8), 461-464.

12. Shao, L.; Yang, Z.-J.; Andrén, D.; Johansson, P.; Käll, M. Gold Nanorod Rotary Motors Driven by Resonant Light Scattering. *ACS Nano* **2015,** *9* (12), 12542-12551.

13. Paterson, L.; MacDonald, M. P.; Arlt, J.; Sibbett, W.; Bryant, P. E.; Dholakia, K. Controlled Rotation of Optically Trapped Microscopic Particles. *Science* **2001,** *292* (5518), 912.

14. Donato, M. G.; Mazzulla, A.; Pagliusi, P.; Magazzù, A.; Hernandez, R. J.; Provenzano, C.; Gucciardi, P. G.; Maragò, O. M.; Cipparrone, G. Light-induced rotations of chiral birefringent microparticles in optical tweezers. *Sci. Rep.* **2016,** *6*, 31977.

15. Reimann, R.; Doderer, M.; Hebestreit, E.; Diehl, R.; Frimmer, M.; Windey, D.; Tebbenjohanns, F.; Novotny, L. GHz Rotation of an Optically Trapped Nanoparticle in Vacuum. *Phys. Rev. Lett.* **2018,** *121* (3), 033602.

16. Quinto-Su, P. A. A microscopic steam engine implemented in an optical tweezer. *Nat. Commun.* **2014,** *5*, 5889.

17. Lu, J.; Li, Q.; Qiu, C.-W.; Hong, Y.; Ghosh, P.; Qiu, M. Nanoscale Lamb wave–driven motors in nonliquid environments. *Sci. Adv.* **2019,** *5* (3), eaau8271.

18. Ndukaife, J. C.; Kildishev, A. V.; Nnanna, A. G. A.; Shalaev, V. M.; Wereley, S. T.; Boltasseva, A. Long-range and rapid transport of individual nano-objects by a hybrid electrothermoplasmonic nanotweezer. *Nat. Nanotechnol.* **2015,** *11*, 53-59.

19. Juan, M. L.; Gordon, R.; Pang, Y.; Eftekhari, F.; Quidant, R. Self-induced back-action optical trapping of dielectric nanoparticles. *Nat. Phys.* **2009,** *5*, 915-919.

20. Zhu, T.; Cao, Y.; Wang, L.; Nie, Z.; Cao, T.; Sun, F.; Jiang, Z.; Nieto-Vesperinas, M.; Liu, Y.; Qiu, C.-W.; Ding, W. Self-Induced Backaction Optical Pulling Force. *Phys. Rev. Lett.* **2018,** *120* (12), 123901.

21. Li, H.; Cao, Y.; Zhou, L.-M.; Xu, X.; Zhu, T.; Shi, Y.; Qiu, C.-W.; Ding, W. Optical pulling forces and their applications. *Adv. Opt. Photon.* **2020,** *12* (2), 288-366.

22. Kajorndejnukul, V.; Ding, W.; Sukhov, S.; Qiu, C.-W.; Dogariu, A. Linear momentum increase and negative optical forces at dielectric interface. *Nat. Photonics* **2013,** *7*, 787-790.

23. Chen, J.; Ng, J.; Lin, Z.; Chan, C. T. Optical pulling force. *Nat. Photonics* **2011,** *5*, 531-534.

24. Gao, D.; Ding, W.; Nieto-Vesperinas, M.; Ding, X.; Rahman, M.; Zhang, T.; Lim, C.; Qiu, C.-W. Optical manipulation from the microscale to the nanoscale: fundamentals, advances and prospects. *Light Sci. Appl* **2017,** *6*, e17039.

25. Novitsky, A.; Qiu, C.-W.; Wang, H. Single Gradientless Light Beam Drags Particles as Tractor Beams. *Phys. Rev. Lett.* **2011,** *107* (20), 203601.

26. Ding, W.; Zhu, T.; Zhou, L.-M.; Qiu, C.-W. Photonic tractor beams: a review. *Adv. Photonics* **2019,** *1* (2), 024001.

27. Martínez, I. A.; Roldán, É.; Dinis, L.; Petrov, D.; Parrondo, J. M. R.; Rica, R. A. Brownian Carnot engine. *Nat. Phys.* **2015,** *12*, 67-70.

28. McCann, L. I.; Dykman, M.; Golding, B. Thermally activated transitions in a bistable three-dimensional optical trap. *Nature* **1999,** *402* (6763), 785-787.

29. Shi, Y.; Zhao, H.; Nguyen, K. T.; Zhang, Y.; Chin, L. K.; Zhu, T.; Yu, Y.; Cai, H.; Yap, P. H.; Liu, P. Y.; et al. Nanophotonic Array-Induced Dynamic Behavior for Label-Free Shape-Selective Bacteria Sieving. *ACS Nano* **2019,** *13* (10), 12070-12080.

30. Pang, Y.; Song, H.; Kim, J. H.; Hou, X.; Cheng, W. Optical trapping of individual human immunodeficiency viruses in culture fluid reveals heterogeneity with single-molecule resolution. *Nat. Nanotechnol.* **2014,** *9* (8), 624-630.

31. Kang, P.; Schein, P.; Serey, X.; O'Dell, D.; Erickson, D. Nanophotonic detection of freely interacting molecules on a single influenza virus. *Sci. Rep.* **2015,** *5* (1), 12087.

32. Yang, A. H. J.; Moore, S. D.; Schmidt, B. S.; Klug, M.; Lipson, M.; Erickson, D. Optical manipulation of nanoparticles and biomolecules in sub-wavelength slot waveguides. *Nature* **2009,** *457* (7225), 71-75.

33. Zhu, X.; Cicek, A.; Li, Y.; Yanik, A. A. Plasmofluidic Microlenses for Label-Free Optical Sorting of Exosomes. *Sci. Rep.* **2019,** *9* (1), 8593.

34. Juan, M. L.; Righini, M.; Quidant, R. Plasmon nano-optical tweezers. *Nat. Photonics* **2011,** *5* (6), 349-356.

35. Chen, X.; Li, T.; Zeng, H.; Hu, Z.; Fu, B. Numerical and experimental investigation on micromixers with serpentine microchannels. *Int. J. Heat Mass Transf.* **2016,** *98*, 131-140.

36. Chen, X.; Li, T. A novel passive micromixer designed by applying an optimization algorithm to the zigzag microchannel. *Chem Eng J* **2017,** *313*, 1406-1414.

FIGURE CAPTIONS:

Figure 1. Design of the automatic cell engine in microfluidics. (a) Schematics of the particle cycle in the optofluidic lattice using a lower laser power. (b) Light pattern and force analysis of a particle pushed away by the optical scattering force using a higher laser power. Different laser powers induce different balance positions in E_2 and E_{22} which will result in different trajectories to cycle back to E_1 or being pushed forward to E_{42}. Brownian force points to all directions. Only the direction from the major hotspot to the major secondary hotspot is plotted here. (c) Energy levels and states of the red particle in (a) from all forces. Solid lines represent the cyclic trajectory of E_1-E_2-E_3-E_4-E_1. Dashed lines represent the trajectory projection in the x-y plane. (d) The energy levels of the green particle in (b) illustrating the trajectory of E_1-E_{22}-E_{32}-E_{42}.

Figure 2. Self-induced back-action (SIBA) optical forces. (a) Illustration of the optical scattering force prevailing over the optical gradient force for the 1-μm particle in the primary hotspot. (b) Optical gradient force dominated pulling for the 100-nm nanoparticle in the primary hotspot. (c) Dominating Forward scatting induced optical pulling force for the 100-nm nanoparticle in the major secondary hotspot. (d) A force equals 0 from the balancing of forward and backward scatting for the 1-μm particle in the major secondary spot. (e) Illustration of two particles (diameter 100 nm and 1 μm) placed in the light pattern and sweeping along the y-direction at x = 11.8 μm. (f) SIBA of optical forces in the x-direction. The forces along the y-direction at x = 11.8 μm are calculated using FDTD and the perturbative methods. (g) Potential wells for the 100-nm and 1-μm particles in the y-direction at x = 11.8 μm. (h) Illustration of two particles (diameter 100 nm and 1 μm) placed in the light pattern and sweeping along the y-direction at x = 16.3 μm. (i) SIBA of optical forces in the x-direction. The forces along the y-direction at x = 16.3 μm are calculated using FDTD and the perturbative methods. (j) The shape of potential well for 100-nm particle by FDTD matches the shape of the light pattern, while, the potential well for the 1-μm particle by FDTD at the main spot region is strongly affected by the SIBA, causing the particle easy to hop into the side potential well. Laser power used in the simulation is 150 mW.

Figure 3. Force and potential analysis for the dynamics of particle inside the asymmetric hotspot landscape. (a) Potential energy calculated from all forces on the 1-μm particle. The contours

indicate the cyclic trajectories of particle. To better show the potential energy landscape and the contour, the landscape is upshifted by 2 k_BT. Calculated overall forces (b) in the *x*-direction and (c) *y*-direction. The force in the *y*-direction combines both the optical and drag forces. Laser power used in (a)-(c) is 300 mW. And the flow velocity is 7 μm/s.

Figure 4. Experimental demonstration of the automatic cell cycle in the microchannel. (a) Schematic illustration of the cycle of an oocyst-particle complex. Video frames demonstrating the cycle movement of (b) a single *Cryptosporidium* oocyst and (c) *Cryptosporidium* oocyst-particle complex. Scale bars equal 5 μm. The oocyst-particle complex has a shorter cyclic range comparing to the single oocyst. Laser power is 100 mW. And flow velocity is approximately 10 μm/s. (d) Recorded *y*-coordinates of the *Cryptosporidium* oocyst indicating the four-stroke process. The period of the engine is 6-7 s. (e) Displacement (blue line) and work (red line) by laser pushing and flow flushing of a single *Cryptosporidium* oocyst in one cycle.

For Table of Contents Use Only

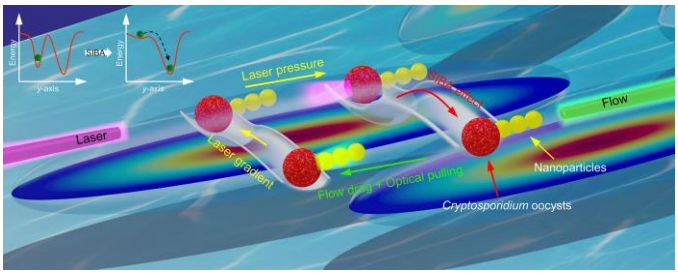

Title: Optofluidic Micro-Engine in A Dynamic Flow Environment via Self-Induced Back-Action

Authors: Yuzhi Shi, Tongtong Zhu, Kim Truc Nguyen, Yi Zhang, Sha Xiong, Peng Huat Yap, Wee Ser, Shubo Wang, Cheng-Wei Qiu, C. T. Chan, and Ai Qun Liu

Brief synopsis: An automatic optofluidic cell engine was built in the microchannel with the synergy of the optical, fluidic and Brownian forces. The self-induced back-action helps to flatten the potential well and generate optical pulling force to realize the microscopic engine.